doi:10.1038/nature10577

Atomic resolution dynamics on the surface of amyloid β protofibrils probed by solution NMR

Nicolas L. Fawzi[1], Jinfa Ying[1], Rodolfo Ghirlando[2], Dennis A. Torchia[3], and G. Marius Clore[1]

Laboratories of Chemical Physics[1] and Molecular Biology[2], National Institute of Diabetes and Digestive and Kidney Diseases, and [3]National Institute of Dental and Craniofacial Research, National Institutes of Health, Bethesda, Maryland 20892-0520, U.S.A.

1. Characterization of protofibrils by atomic force and electron microscopy.

Methods

Atomic force microscopy. Samples for atomic force microscopy (AFM) were prepared as follows. Aliquots were removed from NMR samples incubated for 10 days at 10 °C, diluted by a factor of 5 with deionized water and 20 μl was immediately applied to freshly cleaved mica. After 5 minutes, the excess liquid was removed by blotting the sample edge with filter paper and then washed and immediately blotted twice with 20 μl of deionized water. Samples were then air dried. Tapping mode AFM images were acquired using a MultiMode AFM and Nanoscope IV controller (Veeco, Santa Barbara, CA) equipped with a microactuated silicon probe (Veeco DMASP, 10 nm tip radius, 3 N/m force constant). Images were acquired with a scanning rate of 3 μm/sec.

Electron Microscopy. Negative stain transmission electron microscopy (EM) was carried out exactly as described previously[15]. Briefly, 2.5 μl of an NMR sample (incubated for 10 days at 10°C) was placed on the carbon-coated side of a commercially available carbon film coated copper EM grid (Ultrathin Carbon Film/Holey Carbon, Ted Pella Inc.). After a 5 min adsorption period, solutions were blotted, washed three times with 5 μL deionized water for 5 s and blotted. 5 μL of 3% uranyl acetate was applied for 60 s, blotted, and the sample air-dried. Images were acquired as described by Chen et al.[33]

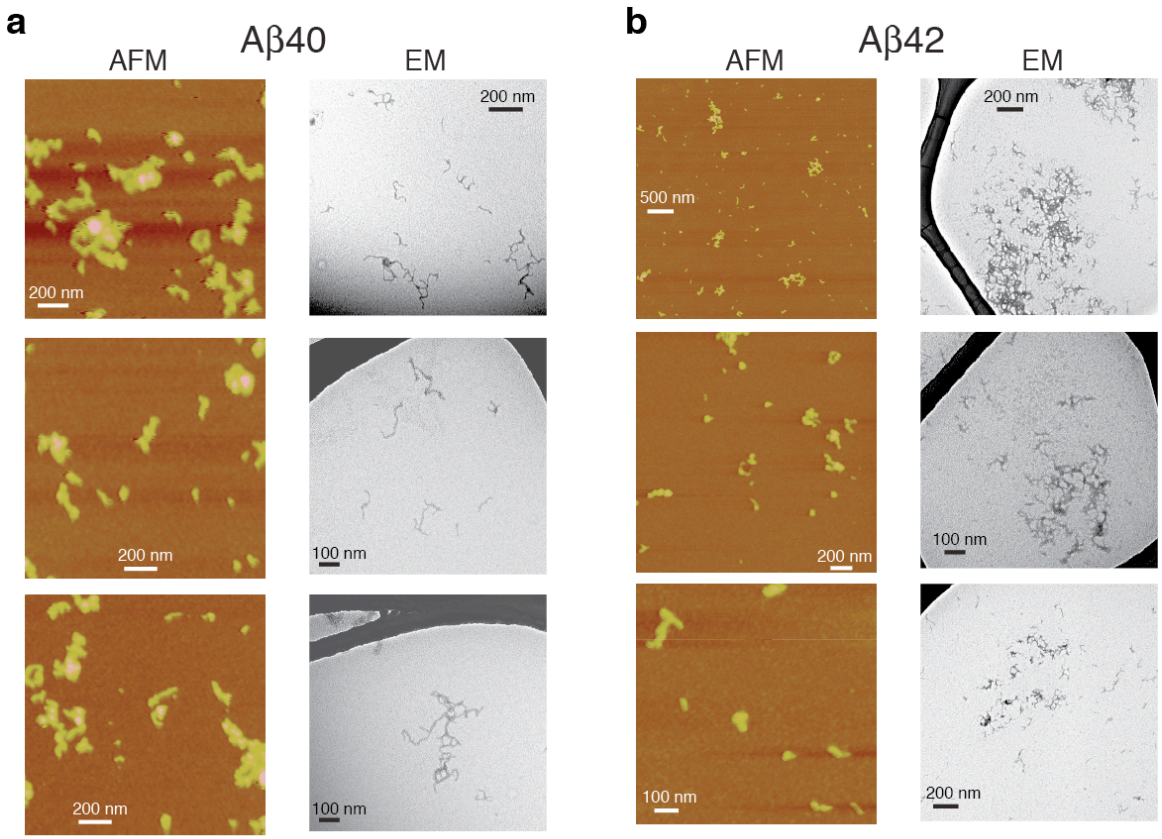

Figure S1 | AFM and EM of protofibrils present in NMR samples. NMR samples of (**a**) 200 μM Aβ40 and (**b**) 160 μM Aβ42 after 10 days of equilibration at 10°C were analyzed by tapping mode AFM and negative stain transmission EM. AFM images (left, colored by height) of Aβ40 and Aβ42 peptides are similar, showing irregularly shaped, worm-like protofibrils with heights of 5 nm for the smallest visible aggregates, up to 10 nm for isolated aggregates, and reaching up to 20 nm for apparent clusters of aggregates. The minimum width of the smallest aggregates seen in the AFM images is ~30 nm, although the width observed by AFM also includes effects of the AFM tip, which has a diameter of ~20 nm. Negative stain EM images (right) of the same samples show the same worm-like protofibrils with widths of ~15 nm and lengths of 50 nm and longer. No amyloid fibrils (defined as straight, unbranched fibers μm in length) are observed in any of the samples. The holey carbon support of the EM grid appears as large dark features on the EM images.

2. Hydrodynamic studies on samples of Aβ40 and Aβ42

Methods

Sample preparation. Samples for sedimentation velocity and dynamic light scattering were prepared and handled in an identical manner to the NMR samples.

***Sedimentation velocity*:** Sedimentation velocity experiments were conducted at 10.0 °C on a Beckman Coulter ProteomeLab XL-I analytical ultracentrifuge. 400 μL of each of the samples were loaded into prechilled 2-channel centerpiece cells and rotor, allowed to equilibrate at 10.0 °C under vacuum for 16–20 hours and then analyzed at either 5 or 50 krpm over a period of 24 - 27 hours. Low speed data were collected using the Rayleigh interference optical detection system at 2 minute intervals. High speed data were collected using both absorbance (230 nm) and interference optical systems with scans collected at 7 minute intervals. Data were analyzed in SEDFIT 12.44[34] in terms a continuous c(*s*) distribution of Lamm equation solutions – high speed data for fresh Aβ42 (50 μM) and Aβ40 (50, 100 μM) were analyzed using an uncorrected *s* range of 0.0 – 10.0 S with a resolution of 200 and a confidence level of 0.68. High speed data for aged Aβ42 (160 μM) and Aβ40 (200, 225 μM) were analyzed in a similar manner using an uncorrected *s* range of 0.0 – 5.0 S with a resolution of 100 and a confidence level of 0.68. In this case, however, only scans from two hours into the run were used in order to remove contributions from large aggregates. Low speed data for aged Aβ42 (160 μM) and Aβ40 (200 μM) were analyzed using an uncorrected *s* range of 0.0 – 250 S with a resolution of 1000 and a confidence level of 0.68. In all cases, excellent fits were obtained with absorbance and interference r.m.s.d. values ranging from 0.0058 – 0.013 A_{230} and 0.0020 – 0.0081 fringes. Solution densities ρ were measured at 10.000°C on an Anton Paar DMA 5000 density meter and solution viscosities η were measured at 10.00°C using an Anton Paar AMVn rolling ball viscometer. The partial specific volumes *v* of Aβ40 and Aβ42 were calculated in SEDNTERP 1.09[35] at 10.0°C and 20.0°C, and corrected for ^{15}N isotopic substitution and partial proton-deuterium exchange. Sedimentation coefficients *s* were corrected to $s_{20,w}$.

***Dynamic light scattering*:** The translational diffusion coefficient *D* was measured from an autocorrelation analysis of quasielastically scattered light. The λ = 514.5 nm emission of an argon ion laser (Lexel, Model 95) was used in the TEM_{00} mode at a constant light intensity with the laser output power adjusted to 150 mW. Autocorrelation functions were accumulated for 5 minutes at 10.0°C and an angle θ of 90° using a Brookhaven Instruments BI-9000 AT autocorrelator with sampling times of 5.0 μs to 100 ms. Data were imported into SEDFIT 12.44 and the normalized intensity autocorrelation functions $g^{(2)}(\tau) - 1$ were used to obtain the second order average decay rate Γ, and moment μ_2 (expressed in terms of the polydispersity μ_2/Γ^2)[36,37]. A CONTIN analysis was also carried out using the Brookhaven Instruments CONTIN program (Version 1.7)[38]– particle diameters, based on the intensity data, were determined in the range of 5 – 500 nm. Hydrodynamic diameters d_h were obtained from the diffusion coefficient *D*, $d_h = kT/3\pi\eta D$, where T is the absolute temperature and η the buffer viscosity.

Results and Discussion

Fresh samples of Aβ40 and Aβ42 are predominantly monomeric at low concentrations – We used sedimentation velocity to characterize samples of freshly prepared Aβ40 and Aβ42. Absorbance and interference experiments carried out at 10.0°C indicate the presence of a major species at 0.74 S along with trace amounts of higher molecular mass aggregates having sedimentation coefficients in the range of 3 to 14 S and possibly higher for Aβ40 at 100 μM (Fig. S2). We do not detect much larger aggregates, as no significant sample losses are observed during the time required to accelerate the sample to 50 krpm. The major species observed for Aβ42 at 50 μM,

representing 99.3% of the total signal, has a sedimentation coefficient of 0.74 ± 0.04 S. Based on the best-fit frictional ratio f/f_o of 1.4, a molecular mass of 5.0 ± 0.6 kDa is estimated thus demonstrating that this represents an Aβ42 monomer (M_{calc} = 4.574 kDa). Trace aggregates observed at 3.5 and 5.3 S, altogether representing less that 0.7% of the total loading material, have estimated masses of ~50 and ~95 kDa, respectively, indicating that no dimers, trimers, tetramers or small oligomeric forms of the peptide are present. Similar observations are made for Aβ40 at nominal loading concentrations of 50 and 100 μM – at 50 μM the major species at 0.73 ± 0.03 S, representing 98.4% of the loading signal has a best-fit molecular mass of 4.6 ± 0.5 kDa; whereas at 100 μM the species at 0.75 ± 0.04 S, representing 97.0% of the loading signal has a best-fit molecular mass of 5.1 ± 0.4 kDa. As in the case of Aβ42, the 0.74 S species represents the Aβ40 monomer (M_{calc} = 4.388 kDa) – aggregates observed at 3.2, 5.2 and 6.9 S have estimated masses of ~50, ~95 and ~140 kDa, respectively, again demonstrating that no small oligomeric species of Aβ40 are observed.

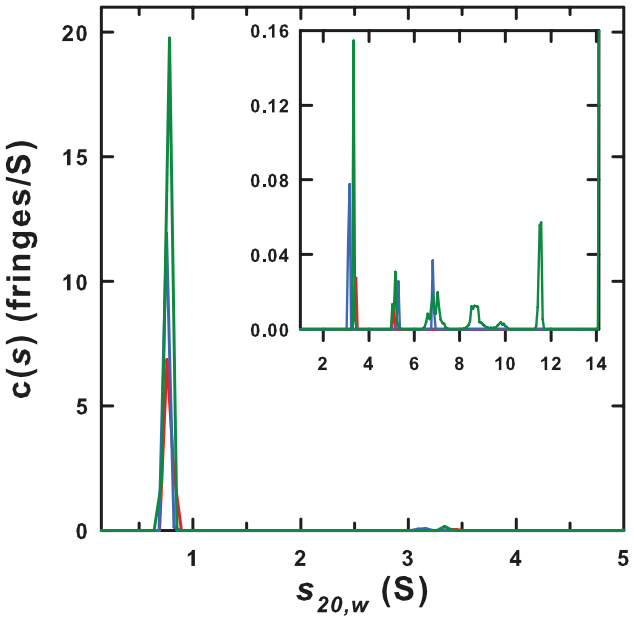

Figure S2 | Aβ40 and Aβ42 are predominantly monomeric at low concentrations. c(*s*) distributions obtained in SEDFIT for fresh solutions of Aβ40 at 50 (blue) and 100 μM (green), as well as 50 μM Aβ42 (red) based on sedimentation velocity interference data collected at 50 krpm and 10.0ºC. The inset highlights traces of high molecular mass aggregates.

Aggregation states of aged Aβ40 and Aβ42 samples at high concentration – Samples of 200 μM Aβ40 and 160 μM Aβ42 were aged for 7 days at 10.0°C. Dynamic light scattering studies carried out just prior to analysis by sedimentation velocity clearly demonstrate the presence of large aggregates (Fig. S3). Autocorrelation functions collected for Aβ40 can be modeled in terms of a distribution of species having an average hydrodynamic diameter of 75 nm and an unusually large polydispersity index of 0.48, consistent with the intensity distribution of hydrodynamic diameters obtained in a CONTIN analysis (Figs S3a and b). Similar observations are made for the aged Aβ42 sample and a second moment cumulant analysis returns an average hydrodynamic diameter of 88 nm and a polydispersity index of 0.43 (Figs. S3c and d). Low speed (5 krpm) sedimentation velocity experiments carried out on these samples were also consistent with a broad distribution of species having sedimentation coefficients ranging from 15 – 200 S (Fig. S4). We note at this stage that the c(*s*) analysis involves direct boundary modeling of the

sedimentation velocity data in terms of a distribution of Lamm equation solutions. To account for boundary broadening due to diffusion, the analysis assumes that all of the sedimenting particles in the distribution have the same frictional ratio f/f_o. An analysis of the low speed sedimentation data returns f/f_o values of 3.1 (Aβ42) and 2.7 (Aβ40) consistent with the presence of asymmetric rod-like particles – based on these values the smallest species at 16.3 S (Aβ42) and 19.2 S (Aβ40) have an estimated molecular mass of 1.8 MDa, indicating that this represents a huge aggregate with a stoichiometry of the order of 400 monomers. Estimated masses for the various aggregates observed range from 1.8 to 85 MDa, leading to species having hydrodynamic diameters of 40 to 160 nm, in qualitative agreement with the observations made by dynamic light scattering. The weight-average sedimentation coefficient of 70.4 S describing the distribution of aggregates observed for the Aβ42 sample corresponds to an average hydrodynamic diameter of 105 nm. Similarly, the weight-average sedimentation coefficient of 56.0 S for Aβ40 corresponds to a hydrodynamic diameter of 74 nm.

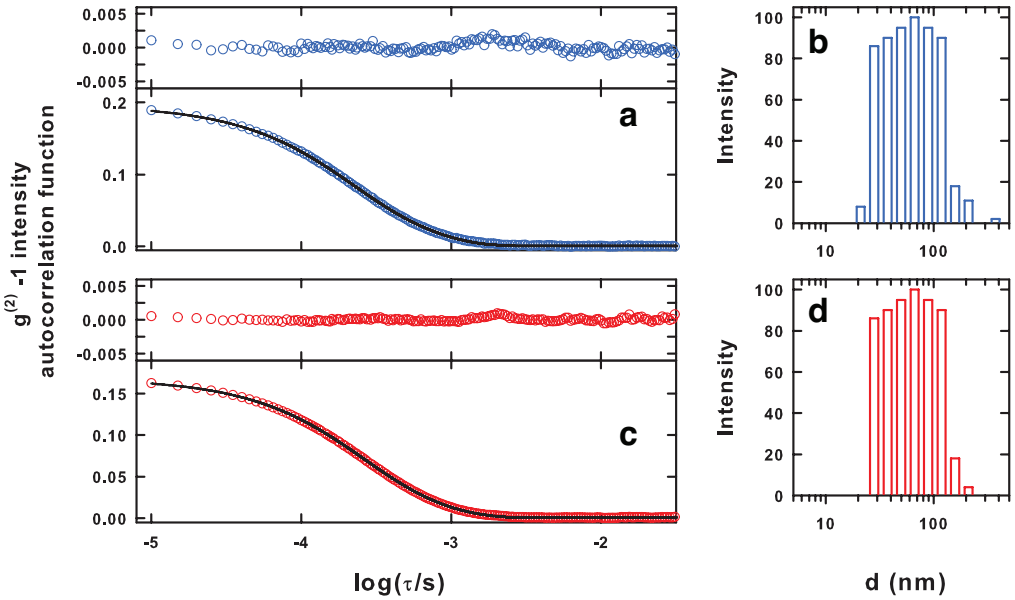

Figure S3 | Aβ40 and Aβ42 form large aggregates at high concentration – light scattering. **a, b**, Dynamic light scattering studies on aged Aβ40 at 200 μM showing the autocorrelation function (**a**) along with the best-fit second moment cumulant and corresponding residuals (d_h = 75 nm and polydispersity = 0.48). **b,** Distribution of hydrodynamic diameters obtained from a CONTIN analysis is also shown. **c, d,** Dynamic light scattering studies on aged Aβ40 at 160 μM showing the autocorrelation function (**c**) along with the best-fit second moment cumulant and corresponding residuals (d_h = 88 nm and polydispersity = 0.43). **d**, Distribution of hydrodynamic diameters obtained from a CONTIN analysis is also shown.

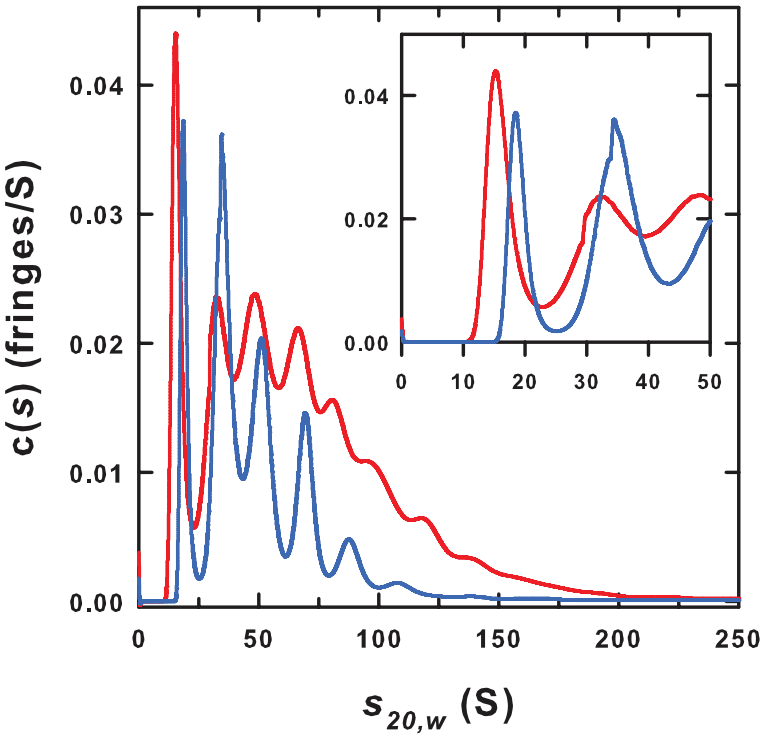

Figure S4 | Aβ40 and Aβ42 form large aggregates at high concentration – sedimentation velocity. c(*s*) distributions obtained in SEDFIT for aged solutions of 200 μM Aβ40 (blue) and 160 μM Aβ42 (red) based on sedimentation velocity interference data collected at 5 krpm and 10.0ºC. The inset highlights the absence of major species below 10 S, noting that data simulation indicates that appreciable quantities of species as small as 5 S would be observed at 5 krpm.

Aged Aβ40 and Aβ42 samples contain significant amounts of monomer – As sedimentation velocity experiments at 5 krpm do not provide any information on the monomeric and possibly small aggregates formed by Aβ40 and Aβ42, we also carried out experiments at 50 krpm. These high speed experiments were carried out using a new batch of aged peptide samples, as well as the samples that were previously characterized by sedimentation at 5 krpm. In the case of the latter, the centrifuge cells containing the sample were shaken in order to resuspend soluble sedimented material. Data analyses were carried out on scans two hours into the run, effectively characterizing species having sedimentation coefficients of 0 up to 10 S. Both samples of Aβ40 showed only peptide monomer at 0.74 ± 0.05 S (Fig. S5a). Essentially identical observations were made for both samples of 160 μM Aβ42 with a species observed at 0.80 ± 0.06 S (Fig. S5b).

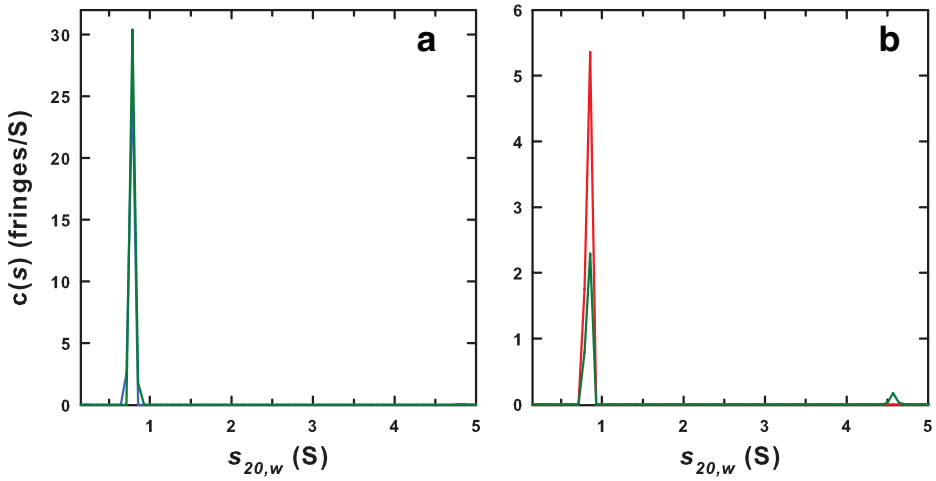

Figure S5 | The presence of Aβ40 and Aβ42 monomers in high concentration solutions – sedimentation velocity. a, c(*s*) distributions obtained in SEDFIT for aged solutions of Aβ40 at 200 μM (blue) and 225 μM (green) based on sedimentation velocity interference data collected at 50 krpm and 10.0ºC. Unlike the aged sample at 225 μM, the sample at 200 μM was previously analyzed by sedimentation velocity at 5 krpm – prior to this high speed analysis, pelleted material was resuspended by shaking the cell. **b,** c(*s*) distributions obtained in SEDFIT for aged solutions of Aβ42 at 160 μM (red, green) based on sedimentation velocity interference data collected at 50 krpm and 10.0ºC. Data shown in red were obtained for a sample that was analyzed by sedimentation velocity at 5 krpm – prior to this high speed analysis pelleted material was resuspended by shaking the cell. The distribution shown in green represents the results obtained for a freshly loaded, aged sample.

In the low concentration sample, the Aβ42 monomer has a sedimentation coefficient of 0.74 S (Fig. S2). Based on this a sedimentation coefficient of ~1.1 S would be expected for an Aβ42 dimer, assuming it had the same overall frictional ratio as the monomer. It is therefore extremely unlikely that the species at 0.80 S in the aged concentrated Aβ42 sample represents a dimer, unless a highly asymmetric and/or unfolded structure is assumed. Moreover, the cross-peaks in the ^{1}H-^{15}N HSQC NMR spectra of the low and high concentration samples are unshifted and the linewidths are only minimally increased (due to the conversion of free monomer to protofibril-bound monomer; see main text), indicating that the NMR visible species in the high concentration sample is identical to that in the low concentration sample, and therefore has to be monomeric.

In conclusion, we have combined sedimentation velocity and dynamic light scattering to characterize preparations of Aβ40 and Aβ42 prepared in the same manner as those used in the NMR DEST and ΔR_2 experiments. At low concentrations, fresh samples of each of the peptides are consistent with the presence of monomeric species, having sedimentation coefficients of 0.74 S. The trace amounts of aggregates observed have sedimentation coefficients consistent with very high molecular mass species. High concentrations of aged peptide samples contain extremely large, asymmetric aggregates characterized by hydrodynamic diameters of 40-160 nm and molecular masses of 1.8-85 MDa, and higher. In addition to these aggregates, high speed sedimentation experiments demonstrate that significant amounts of monomer are still present. Importantly, no intermediate oligomeric aggregates (including dimers, tetramers, octamers) are observed.

3. Dot blot analysis of protofibrils in NMR samples

Dot blot analysis was performed as follows. 2 µl of 200 µM Aβ40 and 160 µM Aβ42 NMR samples, equilibrated for 3 days (high1) and 14 days (high2) at 10°C, were spotted onto nitrocellulose membranes. Membranes were blocked at room temperature in 10% nonfat dry milk dissolved in Tris-buffered saline containing 0.01% Tween 20 (TBS-T) and then probed with polyclonal primary antibodies A11 and OC (gifts of Charles Glabe) at 1 µg/ml and 2.4 µg/ml, respectively, for 1 h. Membranes were thoroughly washed with TBS-T and then incubated with AP-conjugated anti-rabbit secondary antibody (Thermo Scientific) for 45 minutes. The membranes were thoroughly rinsed and antibody binding was detected using CDP-Star® (NEB) chemoluminescent reagent with BioMax Light film (Kodak).

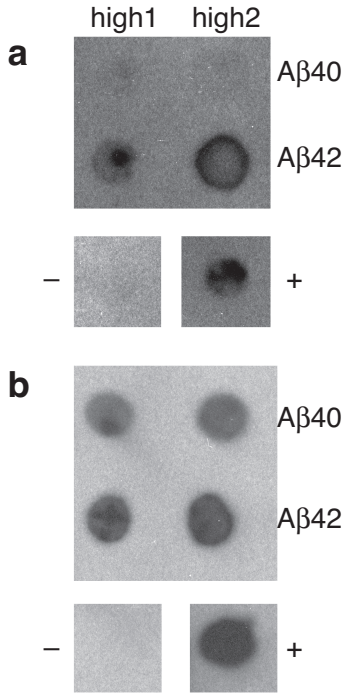

Figure S6 | Dot blot analysis of antibody binding to NMR protofibrils. NMR samples were spotted to nitrocellulose membranes and the binding of (**a**) A11 polyclonal antibody, specific to "pre-fibrillar" oligomers[39], and (**b**) OC polyclonal antibody, specific to "fibrillar" oligomers and fibrils[40], was evaluated. (Note the definition of pre-fibrillar and fibrillar oligomers is based on reactivity towards A11 and OC, respectively[3]). Two high concentration samples (200 µM Aβ40 and 160 µM Aβ42) were tested, one after 3 days (high1), and the other after 14 days (high2) equilibration at 10°C. **a**, Aβ40 samples showed small but detectable binding to A11, while Aβ42 showed significant A11 binding, suggesting that the Aβ42 samples contain more "pre-fibrillar oligomers" than the Aβ40 ones. **b,** Both Aβ40 and Aβ42 samples showed significant binding to OC indicative of the presence of "fibrillar" oligomers. 0.6 mg/ml BSA was used as a negative control (-). A positive control was prepared as described by Kayed et al.[41] by dissolving a lyophilized sample of Aβ42 in 100 mM NaOH to a final concentration of 2.5 mM, diluting to 70 µM in 10 mM sodium phosphate pH 7.4, and followed by incubation for 2 weeks at 4°C. For each antibody binding experiment presented, all images come from the same blot and were processed identically.

4. Supplementary NMR data

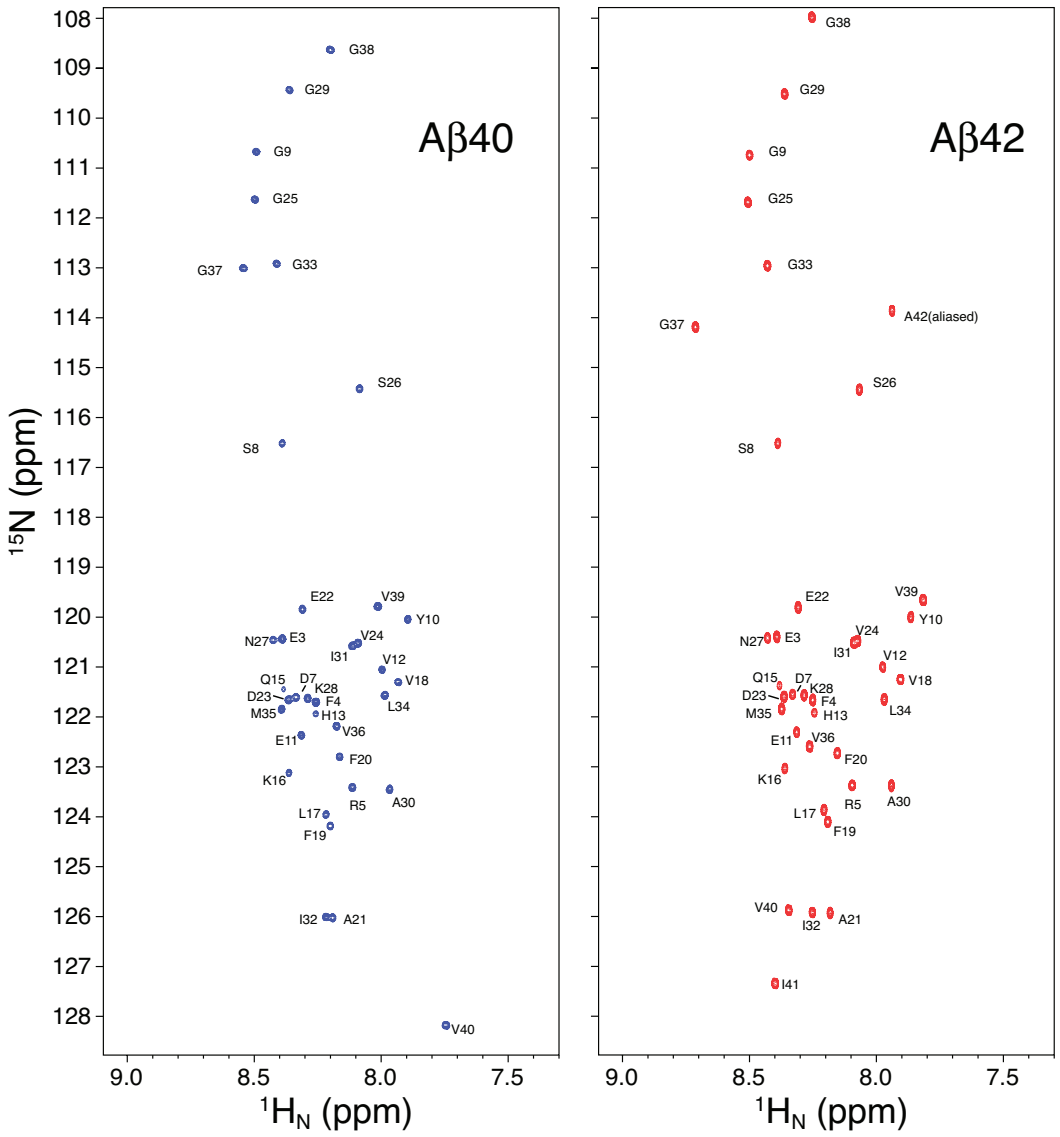

Figure S7 | 900 MHz ^{1}H-^{15}N HSQC spectra of 50 µM ^{15}N-labeled Aβ40 (left) and Aβ42 (right) at 10°C and pH 6.8. As reported previously, Aβ gives excellent spectra under these conditions. For Aβ40, the assignments were transferred from previous studies[19,20] and confirmed by a 3D HNCA triple resonance correlation experiment using an identically prepared sample of ^{15}N/^{13}C-labeled Aβ40 peptide (rPeptide). For Aβ42, the assignments were transferred from the published Aβ42 ^{1}H-^{15}N HSQC spectrum[20] and verified by comparison to the spectrum of Aβ40. For Aβ40 the ^{1}H-^{15}N HSQC spectrum was acquired with 200* × 1900* complex data points in the ^{15}N and ^{1}H dimensions, respectively; for Aβ42 128* × 1900* complex data points were acquired. The spectra of monomeric Aβ40 and Aβ42 are typical of intrinsically disordered peptides. Previous NMR analysis of Aβ40 and Aβ42 indicated that monomeric Aβ was predominantly unstructured and extended with small populations of hydrogen-bonded turns between Asp7-Glu11 and Phe20-Ser26[19].

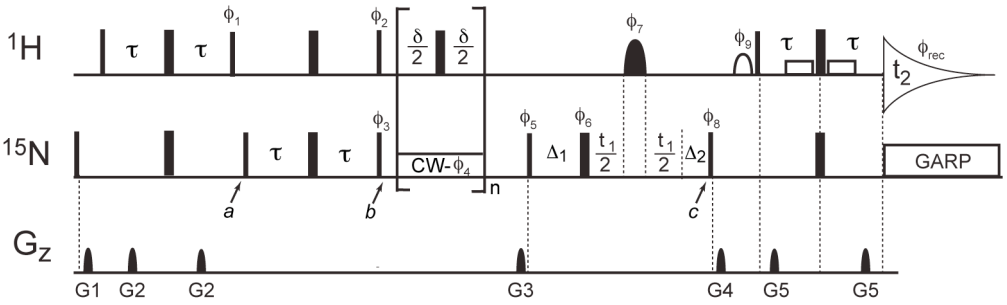

Figure S8 | Pulse sequence for the 2D ^{15}N-*D*ark-state *E*xchange *S*aturation *T*ransfer (DEST) experiment. Narrow and wide filled-in bars represents 90° and 180° pulses, respectively. The filled-in shaped pulse ϕ_7 has an IBURP2 profile[42] with duration 1.4 ms (on a 900 MHz spectrometer) and is applied at 8.25 ppm as an amide proton decoupling pulse. The open shaped pulse (sinc with the central cycle only) and the open rectangular bars represent 1 ms 90° water flip-back pulses. Unless otherwise indicated, all the pulses have phase x; ϕ_1 = y, -y; ϕ_2 = -x; ϕ_3 = y; ϕ_4 = 4(x), 4(-x); ϕ_5 = x; ϕ_6 = 2(x), 2(y), 2(-x), 2(-y); ϕ_7 = 4(x), 4(-x); ϕ_8 = y; ϕ_9 = -x; and ϕ_{rec} = x, -x, -x, x. Quadrature detection in the indirect ^{15}N dimension is achieved using States-TPPI. The G1, G2, G3, G4, and G5 gradient pulses are sine-shaped and have durations of 1.7, 1.7, 1.0, 0.937 and 1.1 ms, respectively. Their corresponding peak powers are 19.6, 2.1, 23.1, 18.9, and 33.6 G/cm along the *z*-axis. Delays: τ = 2.7 ms, $\Delta_1 = \tau$ + PW/2 = 3.4 ms, $\Delta_2 = \tau$ – PW/2 = 2.0 ms, where PW is the width of the IBUPR2 ^{1}H decoupling pulse ϕ_7, and δ = 100 ms. For the saturation experiments, a 0.9 s (i.e. n = 9) ^{15}N CW pulse centered at 15 frequencies (35, 28, 21, 14, 8, 4, 2, 0, -2, -4, -8, -14, -21, -28, and -35 kHz from the carrier 118.5 ppm) is applied at two RF strengths (170 and 350 Hz). In the two reference experiments, the ^{15}N saturation pulse is turned off while application of the 180° ^{1}H pulse train remains active.

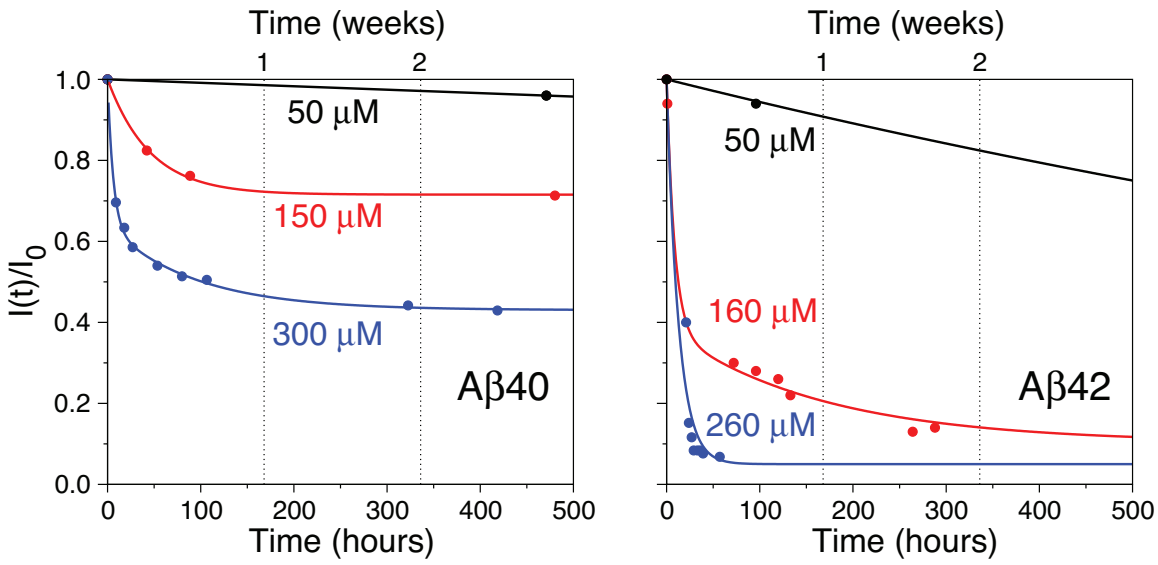

Figure S9 | Timecourse of the integrated intensity of the $^{1}H_{N}$ envelope (measured from the first t_1 increment of a ^{1}H-^{15}N HSQC spectrum) for representative samples of Aβ40 (left) and Aβ42 (right). At a concentration of 50 μM, Aβ40 shows minimal decay and Aβ42 shows a little decay, though no change in ^{15}N-R_2 values are observed within the time range tested for either sample. At higher concentrations, the NMR observable monomer population of Aβ40 decays much less rapidly than that of Aβ42 at similar concentrations. Lines represent double exponential fits to guide the eye. An additional data point for the 50μM Aβ42 sample at 650 hours lies along the fitted curve shown. The data for Aβ40 presented in this figure are from our previous work[14].

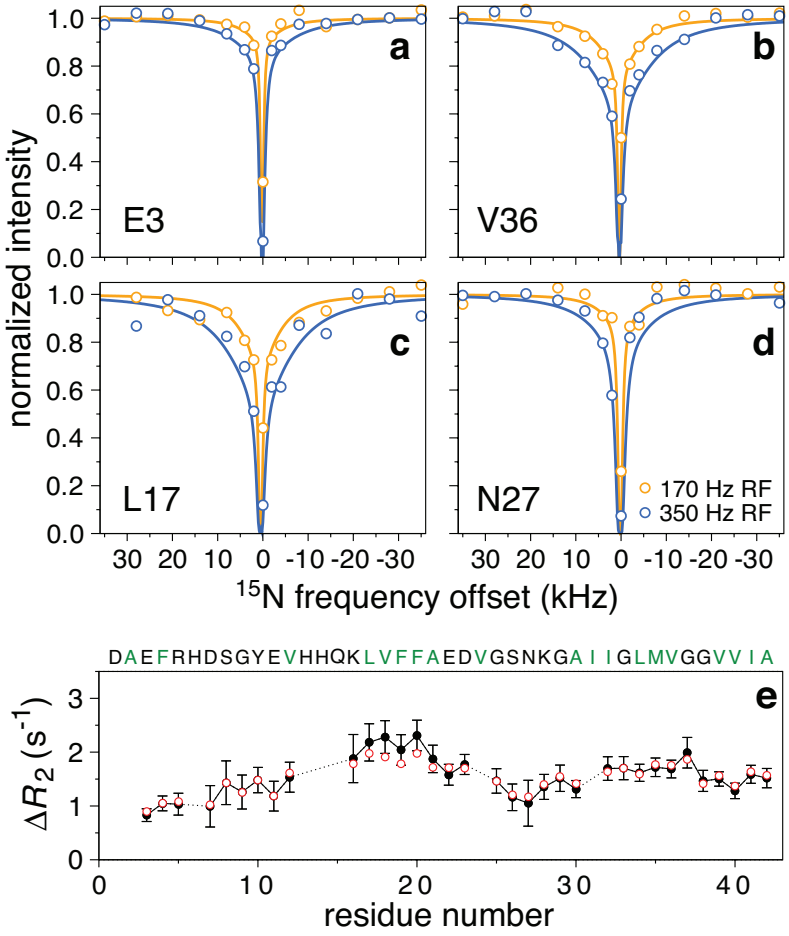

Figure S10 | ^{15}N Dark-state exchange saturation transfer (DEST) and ΔR_2 experiments on Aβ42. DEST profiles showing examples of normalized cross-peak intensities as a function of frequency offset from the ^{15}N carrier frequency (set at 117.6 ppm): **a, b, c** and **d,** Glu-3, Val-36, Leu-17 and Asn-27, respectively, in the 160 μM Aβ42 sample at CW ^{15}N saturation pulse RF field strengths of 170 Hz (orange circles) and 350 Hz (blue circles). The solid lines are the best-fits to an exchange model between monomer free in solution and bound to the surface of the protofibrils incorporating an ensemble of protofibril-bound states in which residues are either tethered or in direct contact with the protofibril surface (cf. Fig. 2b of main text). The standard deviation of the experimental data points is approximately equal to twice the size of the circles. **e**, Observed (black filled-in circles) versus calculated (red open circles) ΔR_2 values for the model in Fig. 2b of the main text. ΔR_2 values are measured as the difference in ^{15}N-R_2 values between the 160 μM sample equilibrated for 1-2 weeks and the predominantly monomeric 50 μM sample. The ^{15}N-R_2 and DEST data for Aβ42 were recorded in the period spanning 1-2 weeks of equilibration: the ^{15}N-R_2 data was recorded first (~18 hrs) followed by the DEST experiment (~5 days), and finally a repeat of the ^{15}N-R_2 data (~18 hrs). The reduced χ^2 values for the simultaneous non-linear least squares best-fit to the DEST profiles and ΔR_2 data is 1.3, indicating that the fit is of similar quality to that of Aβ40 (Fig. 1). Error bars: 1 s.d.

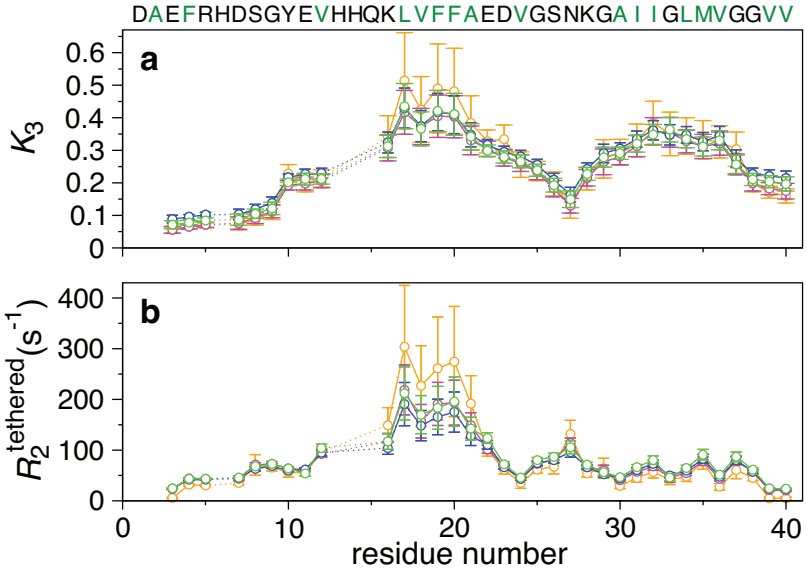

Figure S11 | Comparison of residue-specific calculated parameters describing the ensemble of protofibril-bound states for varying values of the rate constant (k_3) for the conversion of tethered to direct-contact states of Aβ40. The rate constant $k_{-3}(i)$ for the conversion of direct-contact to tethered states is given by $k_3 / K_3(i) = k_3 k_1^{app}(i) / k_2^{app}(i)$, thereby ensuring detailed balance. **a,** Dependence of the residue-specific equilibrium constants, $K_3(i)$, for the relative partitioning of direct-contact to tethered states for the ensemble of protofibril-bound states and **b,** the residue-specific ^{15}N-$R_2^{tethered}$ values for varying values of k_3: k_3 = 0 (blue), 1.8 (green), 10 (magenta) and 40 (orange) s^{-1}. The value of 1.8 s^{-1} is the value of k_3 obtained upon global minimization including k_3 as one of the optimized parameter; for the other cases, k_3 is held fixed at the values indicated during global minimization. The value of $k_3 = 0$ s^{-1} corresponds to that used in the main text and Fig. 3. We note that the introduction of this additional kinetic path is only consistent with the observed data if the rate constant from $I_{tethered}$ to $I_{contact}$ is slow (<< k_{off}). Further, including such interconversion pathways with $I_{tethered}$ to $I_{contact}$ rate constants up to 10 s^{-1} has no significant effect on the fitted parameters and does not improve the fit to the experimental data (Fig. S11 above and Table S1), indicating that tethered and direct-contact states are kinetically separated and that any conformations where residue i is in rapid exchange (>> 10 s^{-1}) between tethered and direct-contact states is counted in $I_{contact}(i)$. Error bars: 1 s.d.

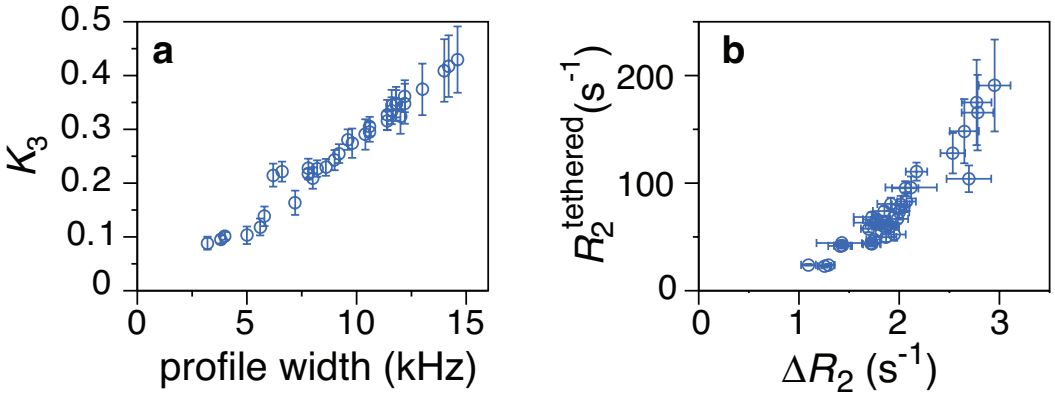

Figure S12 | Correlation between residue-specific fitted parameters and observables for Aβ40. a, Correlation between calculated K_3 values and the width of the experimental ^{15}N-DEST saturation profiles at a normalized intensity of 0.7 (30% attenuation). **b,** Correlation between calculated $^{15}\mathrm{N} - R_2^{tethered}$ and experimental ΔR_2 values. Error bars: 1 s.d

Table S1 | Comparison of reduced χ^2 values from global minimization against the Aβ40 experimental ^{15}N-DEST and ΔR_2 data for varying values of k_3. Reduced χ^2 values for models with different values of the rate constant k_3 for the conversion of tethered to direct-contact states, with a standard deviation of the normalized intensity for the DEST experiment estimated to be 2% (based on the reproducibility of the two control experiments with no saturation). Detailed balance is ensured as described in the legend to Figure S6.

k_3 (s^{-1})	Reduced χ^2
0 (fixed)	1.8
1.8 ± 1.5 (optimized)	1.8
10 (fixed)	2.4
40 (fixed)	3.2
100 (fixed)	4.2

5. Simple explanation of ΔR_2 and DEST experiments and their interpretation

In unstirred solution, the signal intensity of the NMR observable species (in this instance a monomer of Aβ40 or Aβ42, as judged by analytical ultracentrifugation and all NMR criteria) decreases with time (~1 week for Aβ40 and ~2 days for Aβ42) until a pseudo-equilibrium is established which persists for several weeks (Fig. S4). The decrease in signal intensity is due to the conversion of the monomer to large molecular weight, polydisperse protofibrils, as characterized by analytical ultracentrifugation, electron microscopy (EM), atomic force microscopy (AFM) and dynamic light scattering (see above). There is no evidence for the presence of significant amounts of dimers, tetramers or octamers as these would be NMR observable, and no cross-peaks attributable to such species are visible in the ^{1}H-^{15}N HSQC spectra plotted down to the level of the noise. Thus, if such low molecular weight oligomers exist their population must be below the limit of detection, which in this instance is <2%. [Note, the S/N ratios for the monomer cross-peaks in the ^{1}H-^{15}N HSQC spectra are as follows: 120-150:1 and 70-120:1 for the low (50 μM) concentration, monomeric Aβ40 and Aβ42 samples, respectively; 300:1 for the high total concentration 270 μM Aβ40 sample at pseudo-equilibrium which contains ~110 μM monomer; and 75-90:1 for the high total concentration 160 μM Aβ42 sample at pseudo-equilibrium which contains ~35 μM monomer.]

As the concentration of Aβ is raised, there is a small, but measurable increase in the (monomer) NMR signal linewidths (R_2 values), which is close to uniform, displaying only a small but significant variation across the peptide sequence. The usual reason for observing increasing R_2 values under these circumstances is line broadening due to chemical exchange; i.e. exchange between species with different chemical shifts, which typically depends upon the chemical shift differences between the exchanging species, which in turn depends upon nucleus and magnetic field. The R_2 increases (ΔR_2) observed for Aβ, however, are independent of both nucleus and field. The *only* mechanism whereby this can occur involves exchange of monomer with very large molecular weight species, whose NMR linewidths far exceed all differences in chemical shifts between the monomer and the high molecular weight species. This increase in R_2 reflects the unidirectional apparent first order rate constant for the conversion of monomer, free in solution, to monomer bound to the surface of the large molecular weight species (in this case polydisperse high molecular weight protofibrils with a wide range of particle sizes, but all large enough, i.e. M_r > 1 MDa, to ensure rapid decay of magnetization via transverse relaxation when the monomer is bound to their surfaces).

In the DEST experiment, the large R_2 values of the polydisperse NMR invisible species (i.e. the protofibrils) allow for efficient partial saturation by a weak radiofrequency (RF) field even at large offsets where the monomer magnetization is completely unaffected. Partial saturation is transferred to the monomer via chemical exchange and recorded as a decrease in monomer signal intensity. The DEST profiles represent the decrease in signal intensity as a function of RF field offset, and the shape of the profiles are dependent upon the R_2 values of the monomer bound to the surface of the protofibrils. The fact that significant saturation of both ^{1}H and ^{15}N NMR signals is observed when saturation is applied far (>20 kHz) off resonance indicates that the molecular weights of the protofibrils are in excess of 1 MDa. The DEST effect would not be observed for low molecular weight species with much narrower linewidth. The high polydispersity of the protofibrils does not complicate the analysis of the ΔR_2 and DEST data since the parameters that we observe are independent of the protofibril molecular weights when the latter exceed ~1 MDa.

The key to understanding the model presented in Fig. 2b of the main paper lies in the observation that the variations in both ΔR_2 and the DEST profiles are residue specific. This variation cannot be accounted for by simply postulating the existence of lower molecular weight oligomers, since in that case, the ΔR_2 and DEST effects would be uniform throughout the peptide sequence. i.e. there would be *no* sequence variation in ΔR_2 and DEST profiles since each residue

would be subject to the same events and the same average relaxation behavior when bound to the surface of the oligomers. Thus, the only way to explain the sequence variation is one in which there is sequence-dependent variation of tethered and directly-bound states of the monomer bound to the surface of the polydisperse protofibrils (cf Fig. 2b of main text). Since there are many such combinations of states (>>10^6 for Aβ40 and Aβ42), the addition of further variation arising from polydispersity of the protofibrils does not impact the interpretation of the data or its quantitative analysis in terms of the simple model represented in Fig. 2b of the main text.

References

33. Chen, B., Thurber, K. R., Shewmaker, F., Wickner, R. B. & Tycko, R. Measurement of amyloid fibril mass-per-length by tilted-beam transmission electron microscopy. *Proc. Natl. Acad. Sci. U. S. A.* **106**, 14339-14344 (2009).
34. Schuck, P.S. Size distribution analysis of macromolecules by sedimentation velocity ultracentrifugation and Lamm equation modeling. *Biophys. J.* **78**, 1606–1619 (2000). Downloaded from http://www.analyticalultracentrifugation.com/default.htm
35. Hayes, D.B, Laue, T. & Philo, J. http://www.jphilo.mailway.com. Also see Cole, J.L., Lary, J.W., Moody, T.P. & Laue T.M. Analytical ultracentrifugation: sedimentation velocity and sedimentation equilibrium. *Methods in Cell Biol.* **84**, 143-179 (2008).
36. Koppel, D.E. (1972) Analysis of macromolecular polydispersity in intensity correlation spectroscopy: the method of cumulants. *J. Chem. Phys.* **57**, 4814-4820 (1972).
37. Frisken, B.J. (2001) Revisiting the method of cumulants for the analysis of dynamic light-scattering data. *Applied Optics* **40**, 4087-4091 (2001).
38. Provencher, S.W. A constrained regularization method for inverting data represented by linear algebraic or integral equations. *Computer Phys. Commun.* **27**, 213-227 (1982).
39. Kayed, R., Head, E., Thompson, J.L., McIntire, T.M., Milton, S.C., Cotman, C.W. and Glabe CG. Common structure of soluble amyloid oligomers implies common mechanism of pathogenesis. *Science* **300**, 486-489 (2003).
40. Kayed, R., Head, E., Sarsoza, F., Saing, T., Cotman, C.W., Necula, M., Margol, L., We, J., Bredo, L., Thompson, J.L., Rasool,. S., Gurlo, T., Butler, P. & Glabe, C.G. *Molecular Degeneration* **2**, 18 (2007)
41. Kayed, R., Canto, I., Brey, L., Rasool, S., Lukacsovich, T., Wu, J., Albay, R., Pensalfini, A., Yeung, S., Head, E., Marsch, J.L., Glabe, C.G. Conformation depedent monoclonal antibodies distinguish different replicating strains or conformers of prefibrillar Aβ oligomers. *Molecular Degeneration* **5**, 57 (2010).
42. Geen, H., & Freeman, R. Band-Selective Radiofrequency Pulses. *J. Magn. Reson.* **93**, 93-141 (1991)